



# MIT Open Access Articles

## *A 120nW 18.5kHz RC oscillator with comparator offset cancellation for $\pm 0.25\%$ temperature stability*

The MIT Faculty has made this article openly available. **Please share** how this access benefits you. Your story matters.

<b>Citation</b>	Paidimarri, A., D. Griffith, A. Wang, A. P. Chandrakasan, and G. Burra. "A 120nW 18.5kHz RC Oscillator with Comparator Offset Cancellation for $\pm 0.25\%$ Temperature Stability." 2013 IEEE International Solid-State Circuits Conference Digest of Technical Papers (February 2013).
<b>As Published</b>	<a href="http://dx.doi.org/10.1109/ISSCC.2013.6487692">http://dx.doi.org/10.1109/ISSCC.2013.6487692</a>
<b>Publisher</b>	Institute of Electrical and Electronics Engineers (IEEE)
<b>Version</b>	Author's final manuscript
<b>Citable link</b>	<a href="http://hdl.handle.net/1721.1/92830">http://hdl.handle.net/1721.1/92830</a>
<b>Terms of Use</b>	Creative Commons Attribution-Noncommercial-Share Alike
<b>Detailed Terms</b>	<a href="http://creativecommons.org/licenses/by-nc-sa/4.0/">http://creativecommons.org/licenses/by-nc-sa/4.0/</a>

## 10.7 A 120nW 18.5kHz RC Oscillator with Comparator Offset Cancellation for $\pm 0.25\%$ Temperature Stability

Arun Paidimarri<sup>1</sup>, Danielle Griffith<sup>2</sup>, Alice Wang<sup>3</sup>, Anantha Chandrakasan<sup>1</sup> and Gangadhar Burra<sup>2</sup>

<sup>1</sup> Massachusetts Institute of Technology, Cambridge, MA

<sup>2</sup> Texas Instruments, Dallas, TX

<sup>3</sup> MediaTek, Austin, TX

Integrated low-frequency oscillators can replace crystal oscillators as sleep-mode timers to reduce the size and cost of wireless sensors [1]. Since the timer is one of the few continuously functioning circuits, minimizing its power consumption can greatly reduce sleep-mode power of highly duty-cycled systems. Temperature stability of the oscillator is important in order to minimize timing uncertainty and guard time for the radios, and thus maximizing sleep time. The voltage-averaging feedback method described in [2] achieves high stability in the MHz frequencies, but when scaled to the kHz range, requires very large filters. On the other extreme, gate leakage-based timers have been designed for sub-nW power consumption, but operate in the sub-Hz frequencies [3]. In the past, high accuracy RC oscillators in the kHz range have been designed with feedforward correction [1] and self-chopped operation [4]. In this work, an offset cancellation architecture achieves long-term frequency stability and temperature stability while operating at lower power.

The architecture of the proposed offset-cancelling oscillator is shown in Fig. 10.7.1. When phase  $\phi=0$ , a current  $I$  passes through resistor  $R$  to generate a voltage  $I \cdot R$  on node  $V_2$ . At the same time, a matched current source charges capacitor  $C_1$ , such that node  $V_1$  crosses  $V_2$  at time  $RC$ . After  $t_{\text{delay}}$  corresponding to the delay of the comparator and subsequent buffers,  $\phi$  changes to 1, which then resets the capacitor voltage. In addition, the role of the two comparator inputs is reversed, with  $V_1$  being the resistor voltage and  $V_2$  the voltage across capacitor  $C_2$ . The period of the oscillator is thus nominally  $2RC + 2t_{\text{delay}}$ . Two separate capacitors are used in the two phases so that the delay of capacitor discharge is not included in the period. This switching scheme also cancels comparator offset. For example, if the comparator has an offset  $V_{\text{os}}$ , as shown in Fig. 10.7.2, the duration of phase  $\phi=0$  increases by  $CV_{\text{os}}/I$ , however the opposite phase  $\phi=1$  decreases by the same amount, thus the total period of oscillation is constant. This cancellation scheme allows significant power reduction in the oscillator by: (a) permitting low-swing oscillations since offset and temperature variations of the offsets do not proportionally affect frequency stability, (b) requiring only one comparator as opposed to two in traditional architectures, and (c) relaxing the specifications on the comparator offset, and allowing optimization of gain and bandwidth. The offset cancellation also attenuates the effect of flicker noise, improving long-term stability of the oscillator.

In this design  $R$  is chosen to be  $5M\Omega$  and  $C_1$  and  $C_2$  are  $5pF$  for an RC time constant of  $25\mu s$ . The charging current  $I$  is  $30nA$  on each branch, for a swing of only  $150mV$ . Simulations show that a  $10mV$  offset change ( $\sim 6\%$  of the swing) affects the frequency by only  $0.06\%$  thanks the offset cancellation scheme, a  $100x$  improvement.

Temperature stability of the oscillator is affected by the on-resistance and off-leakage of switches  $S_1$ - $S_6$  in addition to comparator delay variations. For example, resistance changes of  $5k\Omega$  or leakage current variations of  $30pA$  change the oscillation frequency by  $0.1\%$ . The switch size is optimized by considering that large devices give low on-resistance while smaller devices give lower leakage. For example, discharging switches  $S_5$ ,  $S_6$  are sized weak since the discharge delay does not affect frequency. Switches  $S_3$ ,  $S_4$ , when off, see a  $V_{\text{GS}}$  of  $-150mV$ , decreasing leakage by  $>30x$ , and are hence sized for resistance.

The comparator and Schmitt trigger design is shown in Fig. 10.7.3. In order to handle low common-mode inputs, a PMOS-input design is used and saturation of the input pair is ensured by sub-threshold operation. Transconductance efficiency ( $g_m/I_d$ ) is also maximized, hence reducing power. The bandwidth of the comparator is set such that its delay is about  $100ns$ ,  $<0.4\%$  of the period. In addition, to keep the comparator delay independent of temperature, a PTAT current reference is used, ensuring constant  $g_m$  in sub-threshold, which in turn gives constant bandwidth. During the change of phase, when nodes  $V_1$  and  $V_2$  switch roles, the comparator has small voltage glitches, which may result in rail-

to-rail glitches at the output of the inverters. In order to prevent these glitches, and limit cycling, the first buffer stage connected to the comparator is a Schmitt trigger, implemented in a digital fashion. A small hysteresis minimizes asymmetry in the switching point of the comparator in the two phases. Weak high-VT transistors provide a hysteresis of a few  $10s$  of  $mV$ , which is still sufficient to eliminate glitches. The Schmitt trigger and subsequent inverters add  $<10ns$  to the overall delay, and hence do not affect temperature stability of the oscillator.

The oscillator was fabricated in a  $65nm$  CMOS process. The die photo is shown in Fig. 10.7.7. The RC oscillator consumes an area of  $0.032mm^2$ . The oscillator operates from a  $1V$  supply and consumes  $120nW$ . The current sources charging  $R$  and  $C$  consume  $30nA$  each, the comparator  $40nA$ , current mirrors  $10nA$  and the Schmitt triggers and buffers consume  $10nA$ . The current reference, shared with the rest of the system, works from a system supply voltage of  $1.5V$ - $3.3V$  and consumes  $25nA$ . It generates the  $10nA$  PTAT current reference required for the oscillator. The center frequency is tunable from  $9$  to  $30kHz$  through on-chip  $R$  and  $C$  tuning. All measurements described further are at the center of this range ( $\sim 18.5kHz$ ). The oscillator has a supply voltage dependence of less than  $1\%/V$ , allowing relaxed supply regulation requirements.

Temperature stability measurements are shown in Fig. 10.7.4. Over  $-40$  to  $90^\circ C$ , the oscillator has a frequency variation of  $\pm 0.25\%$ . In a reduced temperature range from  $0$  to  $90^\circ C$ , the frequency variation reduces to  $\pm 0.1\%$  for an average of about  $22ppm/^\circ C$ . The effect of offset compensation is also demonstrated by comparing temperature stability of the total period with the period of one of the phases. Offset cancellation achieves a  $7x$  reduction from  $\pm 1.8\%$  down to  $\pm 0.25\%$ . The effect of charging current values is characterized by comparing two charging currents,  $20nA$  and  $30nA$ . At  $20nA$ , switch leakage and reduced slope on the capacitor charging degrades performance giving  $\pm 0.5\%$  temperature variation. The total oscillator current consumption as a function of temperature is also plotted in Fig. 10.7.4.

Long term stability of the oscillator is also critical to sleep-mode timer performance, and is captured by the Allan deviation, plotted in Fig. 10.7.5 for a  $24hr$  measurement in a typical office environment. At averaging times below  $0.5s$ , it is white noise limited; and beyond this, it is flicker noise limited. The offset-cancellation scheme helps reduce the flicker noise and its contribution to the Allan deviation, leaving a floor below  $20ppm$  for intervals over  $0.5s$ . This indicates the ability of the oscillator to measure long sleep times accurately. Fig. 10.7.6 summarizes this work and compares it with previously published RC oscillators operating in various frequencies.

In conclusion, an offset cancellation scheme has been presented that helps achieve temperature stability of  $\pm 0.25\%$ , ultra-low power operation at  $120nW$  and long-term stability of better than  $20ppm$ , advancing the state of fully-integrated timers for wireless sensors.

**Acknowledgements:** The authors would like to acknowledge P. Roine and P. Nadeau for useful discussion and J. Reid for skilled layout.

### References:

- [1] T. Tokairin, et al., "A  $280nW$ ,  $100kHz$ , 1-cycle start-up time, on-chip CMOS relaxation oscillator employing a feedforward period control scheme," *Dig. Symp. VLSI Circuits*, pp. 16-17, June 2012
- [2] Y. Tokunaga, et al., "An on-chip CMOS relaxation oscillator with power averaging feedback using a reference proportional to supply voltage," *ISSCC Dig. Tech. Papers*, pp. 404-405, Feb. 2009
- [3] Y. Lee, et al., "A  $660pW$  multi-stage temperature-compensated timer for ultra-low-power wireless sensor node synchronization," *ISSCC Dig. Tech. Papers*, pp. 46-48, Feb. 2011
- [4] K.-J. Hsiao, "A  $32.4 ppm/^\circ C$   $3.2$ - $1.6V$  self-chopped relaxation oscillator with adaptive supply generation," *Dig. Symp VLSI Circuits*, pp. 14-15, June 2012
- [5] K. Choe, et al., "A precision relaxation oscillator with a self-clocked offset-cancellation scheme for implantable biomedical SoCs," *ISSCC Dig. Tech. Papers* pp.402-403, Feb. 2009
- [6] J. Lim, K. Lee, K. Cho, "Ultra low power RC oscillator for system wake-up using highly precise auto-calibration technique," *ESSCIRC, 2010 Proceedings of the*, pp.274-277, Sept. 2010
- [7] F. Sebastiano, et al., "A Low-Voltage Mobility-Based Frequency Reference for Crystal-Less ULP Radios," *J. Solid State Circuits*, vol.44, pp.2002-2009, July 2009

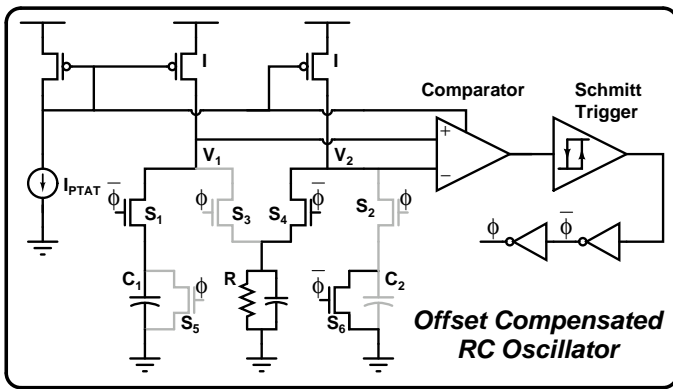


Figure 10.7.1: Architecture of the proposed offset compensated RC oscillator. The switch state for phase  $\phi=0$  is shown with off switches grayed out.

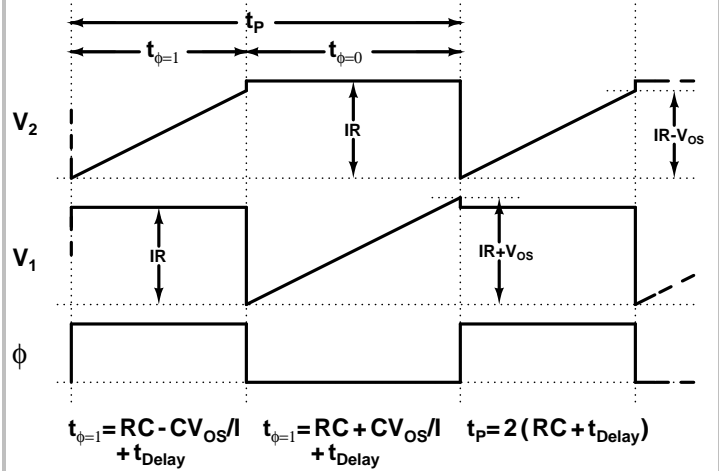


Figure 10.7.2: Timing diagram showing the operation of the offset-cancellation architecture for the case of positive comparator offset  $V_{OS}$ .

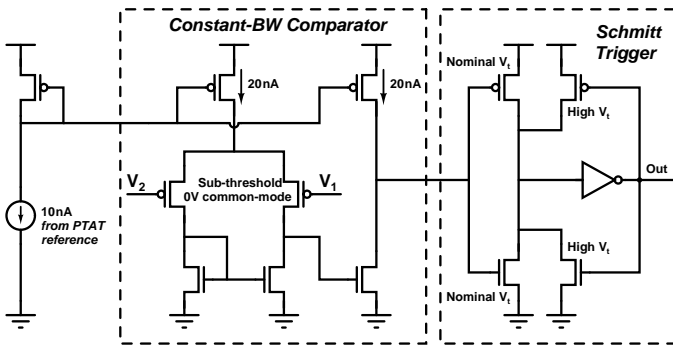


Figure 10.7.3: Implementation of the constant-BW comparator and the digital Schmitt trigger.

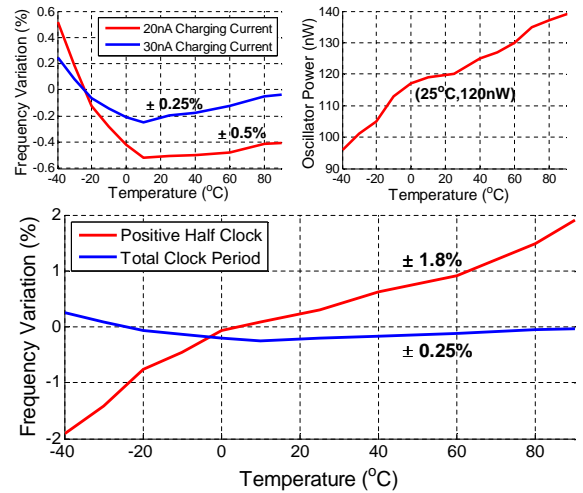


Figure 10.7.4: Temperature measurements for the oscillator showing the effect of varying charging current, total power consumption and effectiveness of the offset compensation scheme.

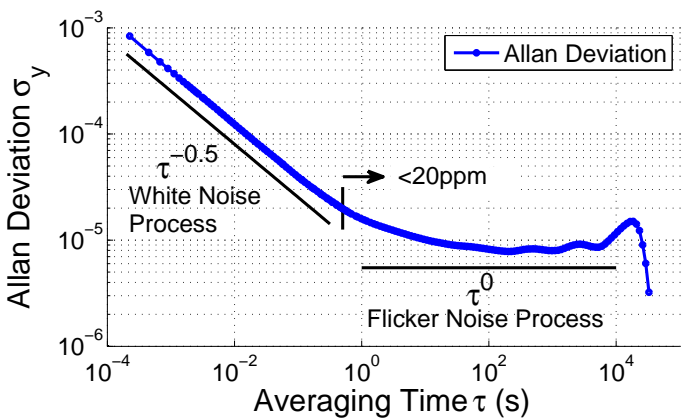


Figure 10.7.5: Allan Deviation measurement over 24 hours shows long-term stability of the oscillator.

Ref	Process	Area (mm <sup>2</sup> )	Freq (kHz)	Power (μW)	Temp Accuracy	Temp Range (°C)	Voltage Accuracy
[1] VLSI'12	90nm	0.12	100	0.28	± 0.68%	-40 to 90	5.7%/V
[2] ISSCC'09	0.18μm	0.04	14000	45	± 0.19 %	-40 to 125	1.6%/V
[3] ISSCC'11	0.13μm	0.01	0.00037	0.00066	± 0.14%	-20 to 60	-
[4] VLSI'12	60nm	0.048	32.768	4.48	± 0.1%	-20 to 100	0.06%/V
[5] ISSCC'09	0.13μm	0.073	3200	38.2	± 0.25%	20 to 60	4%/V
[6] ESSCIRC'10	0.18μm	0.016	31.25	0.36	0.4%/C	-	5%/V
[7] JSSC'09	65nm	0.11	100	20.8	± 1.1%	-22 to 85	2.3%/V
This Work	65nm	0.032	18.5	0.120	± 0.1%	0 to 90	1%/V
					± 0.25%	-40 to 90	

Figure 10.7.6: Summary of measured results and comparison to previous work.

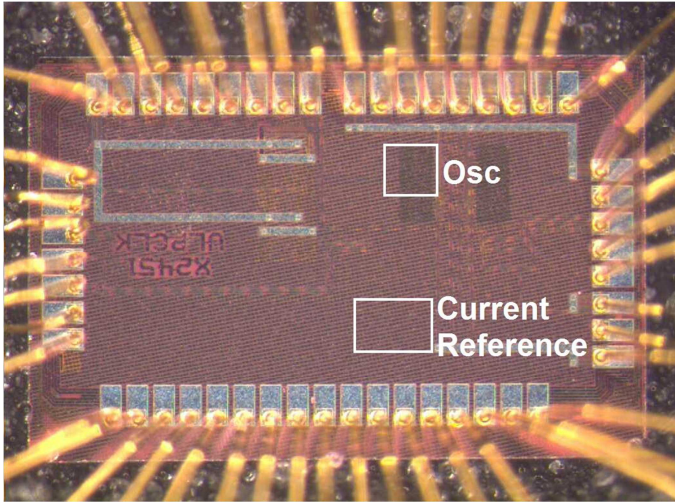


Figure 10.7.7: Die photo of the chip fabricated in 65nm CMOS.